Ferritin-Mediated siRNA Delivery and Gene Silencing in Human Tumor and Primary Cells

Le Li [a,b], *Maider Muñoz Culla* [c], *Unai Carmona* [a,b], *Maria Paz Lopez* [d], *Fan Yang* [a], *Cesar Triguero* [d], *David Otaegui* [c], *Lianbing Zhang* [a,b,*], *and Mato Knez* [b,e,*]

[a] School of Life Sciences, Northwestern Polytechnical University, 710072 Xi'an, China
[b] CIC nanoGUNE, Tolosa Hiribidea 76, 20018 Donostia-San Sebastian, Spain
[c] Biodonostia Health Research Institute, 20014 Donostia-San Sebastian, Spain
[d] Fundación Inbiomed, Paseo Mikeletegi 81, 20009 Donostia-San Sebastian, Spain
[e] IKERBASQUE, Basque Foundation for Science, Maria Diaz de Haro 3, 48013 Bilbao, Spain
* Corresponding authors, E-mail: l.zhang@nanogune.eu; m.knez@nanogune.eu

Abstract: We demonstrate a straightforward method to encapsulate siRNA into naturally available and unmodified human apoferritin. The encapsulation into apoferritin is independent of the sequence of the siRNA and provides superior protection for those sensitive molecules. High efficiency in transfection can be achieved in human tumorigenic cells, human primary mesenchymal stem cells (hMSC) and peripheral blood mononuclear cells (PBMCs). In contrast to Lipofectamine, highly effective gene silencing can be achieved with ferritin as the delivery agent in both tumor cells and PBMCs at low siRNA concentrations (10 nM). As an endogenous delivery agent, apoferritin does not induce immune activation of T- and B-cells in human PBMCs. Apoferritin shows intrinsic anti-inflammatory effects and apoferritin-mediated delivery shows a preference for immune-activated T- and B-cells, a natural selectivity which may turn useful for drug delivery in case of infections or inflammatory diseases.

Key Words: siRNA; ferritin; primary cells; gene silencing; drug delivery

Introduction

Drugs that are based on nucleic acids, including small interfering RNA (siRNA), are gaining importance for their demonstrated remarkable efficiency in the treatments of a variety of diseases [1,2]. The benefit of siRNA for a use as a drug lies in the possibility of designing the molecule to target any gene with a very high level of specificity [3,4]. However, numerous

obstacles are present that affect the in vitro and in vivo use of siRNA [5, 6]. In contrast to DNA, RNA molecules suffer from limited stability and unprotected siRNA will be subject of enzymatic degradation in the bloodstream, thereby limiting its systemic exposure in clinical use [7]. Furthermore, the negative electrostatic charge of siRNA prevents its binding to the cell membrane and the translocation into the cytoplasm. Obviously, a successful application of siRNA in vitro or in vivo is strongly dependent on the delivery system, which witnesses great attention of the researchers in both development and optimization.

In spite of the effort invested until now, all popular delivery agents have serious issues that restrict their straightforward use for siRNA delivery [5-8]. On one hand there are viral vehicles that, besides their inherent safety concerns, cannot deliver siRNA directly into the cell. On the other hand, non-viral delivery agents either show lower efficiency or are toxic for the cells, which is often due to their synthetic nature [8-10]. Some of the methods that work with immortalized cell lines often fail with the very delicate primary cells. Even with immortalized cell lines, all described chemical delivery methods suffer from poor performance with cells in suspension [11]. All those issues present obstinate problems for both laboratory routine and clinical gene therapy.

In order to circumvent the obstacles imposed by delivery vehicles that are composed of exogenous materials, application of endogenous cellular components lately became a new delivery concept. Of particular interest are materials that are involved in cellular uptake pathways and intrinsically show biological functionalities that permit easy passage through cellular membranes without harm [12,13]. Prominent examples include isolated exosomes with genetically engineered modifications that have been investigated as natural counterparts of synthetic liposomes for gene delivery [14-16]. In this case, the limitations for an application on a large scale are related to the low availability of exosomes in quantities, for which the natural production and isolation of the exosomes is the bottleneck [17].

Human ferritin or apoferritin (demineralized form of ferritin) are not affected by such limitations, which is one of the reasons for their rising popularity as promising alternative delivery agent. This molecular complex is formed through an assembly of two subunits of ferritin, the heavy chain (H-chain) and light chain (L-chain) proteins, which comprise a cage-like structure with a hollow cavity of 8 nm in diameter. Naturally, it is used for storage of iron in form of ferrihydrite [18]. Demineralization of ferrihydrite results in a cavity that provides space for loading molecular cargos that will be camouflaged and protected by the surrounding protein cage. The natural cellular uptake of ferritin provides a biological pathway to facilitate cellular delivery of any cargo loaded into the cavity through receptor-mediated endocytosis [19]. Together with its ease of handling, ferritin became popular in material science and biomedicine as template for synthesis or as delivery vehicle for various nanomaterials, anticancer drugs and so on [19-25]. In earlier approaches, genetically engineered ferritin has been used as substrate for binding siRNA to its outer surface [26]. Instead of a cellular uptake of ferritin, the siRNA delivery in the mentioned work is mediated by an additional tumor targeting and cell penetrating peptide.

In this work, we show for the first time that various siRNA molecules can be easily encapsulated into unmodified human apoferritin independent of their sequence. siRNA molecules with an overall size of 20-24 nucleotides can in principle target any gene, if synthesized with an appropriate sequence. Loaded inside the cavity of apoferritin, siRNAs will become protected from enzymatic degradation and therefore will gain great environmental stability. Furthermore, autogenic human apoferritin enables efficient delivery of the encapsulated siRNA not only to human cancer cell lines, but also to human mesenchymal stem cells (hMSC) and to human primary T-cells in suspension.

Materials and Methods

Recombinant human H- and L-apoferritin was purchased from MoliRom, Italy. All siRNA molecules were purchased from Lifetechnologies (Thermo Scientific). All chemicals used in this work were purchased from Sigma-Aldrich unless stated otherwise. The UV-vis absorption was measured with the NanoDrop 2000c (Thermo Scientific).

siRNA encapsulation and agarose gel electrophoresis

The siRNA encapsulation followed the disassembly-reassembly procedure published elsewhere[19]. Briefly, the disassembly of apoferritin (H or L) was achieved by lowering the pH value of apoferritin solution (150 mM NaCl) to 2 with HCl. Disassembled apoferritin was then added to 0.04 nmol siRNA solution which was previously mixed with 20x borate buffer having a pH value of 8.5. Different amounts of apoferritin were used: 0.12 nmol, 0.2 nmol, and 0.4 nmol, resulting in different molar ratios of siRNA and apoFt (1:3, 1:5, 1:10). The reassembled apoferritin-siRNA was stored on ice until use.

Reassembled apoFt with siRNA (H-siRNA or L-siRNA) was treated with 0.5 µg/ml RNase A at 37ºC for 30 min, followed by a treatment with 0.5 mg/ml Proteinase K at 37ºC for 30 min. RNase A digested all free siRNA outside of apoFt and Proteinase K degraded the RNase. An identical amount of bare siRNA was used as control. All samples were then incubated with RNA-loading buffer and loaded in 1% agarose gel. The siRNA in agarose gel was visualized using a KODAK imager. The quantification of the signal intensity was carried out with the Image Studio software (LiCor Bioscience).

Zeta potential and size distribution

The Zetasizer ZS (Malvern) was used to measure the zeta potential based on the laser doppler micro-electrophoresis and the size distribution based on the dynamic light scattering. With this method, an electric field is applied to a solution of molecules or a dispersion of particles, which then move with a velocity related to their zeta potential. This enables the calculation of electrophoretic mobility, and from this mobility the zeta potential and zeta potential distribution

can be derived. By the measurements the pH value of the apoferritin solutions (150 mM NaCl) was adjusted with diluted NaOH or HCl.

Native polyacrylamide gel electrophoresis (Native PAGE):

Continuous native PAGE was used to analyze the stability of the protein. Tris/Boric acid buffer (50 mM Tris, 25 mM boric acid, pH 8.7) was used for the gel formation and as the running buffer. siRNA-apoferritin samples were mixed in 1:1 ratio with the sample buffer (10% Tris/Boric acid buffer, with 30% glycerol, 2% bromophenol blue (0.5%) and separated with a continuous 4% native gel. Following with the PAGE, the gel was stained with Imperial™ Protein Stain (Thermo Scientific).

Cell culture

The human colon adenocarcinoma cell line Caco-2 originated from the European Collection of Cell Cultures (Sigma-Aldrich, Spain). Cells (passages 26-52) were cultured in minimum essential medium (MEM) supplemented with 10% fetal bovine serum (FBS) (Biochrom), 1% nonessential amino acids and 50 μg/mL gentamicin. The culture medium was replaced 1 d after seeding, then every 2 d, and 1 d before the assay.

The human liver carcinoma cell line HepG2 was obtained from the American Type Culture Collection (ATCC, No. HB-8065). Cells between passages 6-19 were used for the experiments. The cells were maintained in MEM supplemented with 10% FBS, 1 mM pyruvate, 1% nonessential amino acids and 50 $\mu g\ mL^{-1}$ gentamicin. For the assays, HepG2 cells were cultured for 3 d with the culture medium having been replaced every day.

The cell viability was determined with the cell counting kit-8 (CCK-8) according to the manufacturer's protocol. The absorbance at 450 nm was measured with a plate-reader (Victor X5, PerkinElmer).

Cellular InsR-silencing with siRNA and total cell lysate preparation

In these experiments siRNA against InsR were used for encapsulation. By the encapsulation the molar ration of siRNA/apoferritin was 1:5. After encapsulation, the samples were passed

though desalting columns with a molecular cutoff of 40 kDa to remove free siRNA. The cells were 50-70% confluent on the day of transfection. 10 nM bare or apoferritin-encapsulated siRNA for Caco2 cells (25 nM for HepG2 cells) was added directly to the freshly changed medium and incubated for further 12 h. Lipofectamine 3000-siRNA was prepared with the commercial Lipofectamine 3000 Transfection Reagent (Invitrogene, Thermo Scientific) according to the instruction. After 12 h incubation time the cells were washed twice with cold PBS and the total cell lysates were harvested with the RIPA buffer (Thermo Scientific). The proteins in the total lysate were analyzed with Western Blots.

Confocal microscopy of cellular Cy3-siRNA transfection

Cells were cultured in 35 mm petri dishes and grown to approximately 60-70 % confluence. Cy3-siRNA encapsulated in apo-huFH with a final concentration of 350 nM was added to the media. After 4 h incubation time the cell nuclei were stained with 10 µg/ml DAPI for 10 min. Subsequently, the cells were washed twice with cold PBS and changed with a live cell imaging solution (Gibco). Living images of cells were acquired with an argon ion UV laser for excitation and emissions of Cy3-siRNA(Ex/Em: 550/570-580 nm, red). The samples were examined with a laser scanning confocal microscope (Zeiss LSM 710) and imaged with a 63× objective. The lines from an argon ion UV laser were used separately for excitation. The channel sequential scanning mode was used. During the imaging period (ca. 2 h) the alignment was kept constant.

Lysosomal Detection

Cells were cultured in 35 mm petri dishes and grown to approximately 30-50 % confluence. FITC-siRNA encapsulated in apo-huFH with a final concentration of 50 nM was added to the media. After 15 min. or 24 h incubation time the cells were washed with PBS and added 1 ml of new medium. Lysosomes were detected with Lyso-ID Lysosomal Detection Kit (Enzo Life Sciencies). Briefly, 1 µl Lyso-ID red dye and 1 µl Hoechst 33324 from the kit were added to 1 ml cell medium. Subsequently, the cells were incubated in dark for 15 min. For imaging, the cells were washed twice with cold PBS and changed with a live cell imaging solution (Gibco).

For the positive control, the cells were pre-incubated with 150 μM chloroquine for 2h before the lysosomal detection. Living images of cells were acquired with an argon ion UV laser for excitation and emissions of FITC (Ex/Em: 498/518 nm), Lyso-ID red dye (Ex/Em: 550/670 nm) and Hoechst (Ex/Em: 350/450 nm). The samples were examined with the laser scanning confocal microscope (Zeiss LSM 710) and imaged with a 63× objective. The lines from an argon ion UV laser were used separately for excitation. The channel sequential scanning mode was used. During the imaging period the alignment was kept constant.

Human peripheral blood mononuclear cells (PBMCs)

PBMC for the experiments of 10 and 25 nM siRNA delivery were isolated from peripheral blood collected in sodium heparin tubes (Vacutainer, Becton Dickinson) using the Ficoll-Hypaque density gradient method within 2 hours of sampling. Cells were cultured in RPMI medium 1640 with L-Glutamine (Gibco, Thermo Fisher) supplemented with 10% fetal bovine serum, 10,000 U/ml penicillin, 10,000 μg/ml streptomycin. For the stimulation of cells phytohemagglutinin (PHA) (Gibco, Thermo Fisher) was used at 0.5%. Cells were incubated at 37°C and 5% CO_2. After incubation cultured PBMCs were harvested, washed with PBS and incubated with antibodies for 20 minutes at room temperature in darkness. Afterwards, cells were washed with PBS and analyzed in a Guava EasyCyte 8HT flow cytometer (Millipore) using the InCyte software v2.2.2. Cell viability was assessed with 7-aminoactinomycin D (7-AAD) (Molecular Probes), cell activation, T and B cells were determined measuring the expression of CD25, CD3 and CD19, respectively using the following antibodies: PE-conjugated anti-human CD25, FITC-conjugated anti-human CD3 and APC-conjugated anti-human CD19 (BD Pharmingen™).

Protein detection with Western Blot analysis

The cells were washed twice with ice-cold PBS. The total lysate of cells was collected with the RIPA buffer (Thermo Scientific). The total protein concentration of the fractions was measured with the BCA assay (Thermo Scientific). Electrophoresis was carried on with 4-20% gradient

Tris-glycine polyacrylamide gels for SDS-PAGE (Thermo Scientific) and electroblotted onto polyvinylidene fluoride (PVDF) (BioRad). PVDF membranes were blocked for 2 h at room temperature in 5% BSA–Tris-buffered saline/Tween 20 (TBST; 25 mM Tris HCl, pH 7.5/150 mM NaCl/0.05% Tween 20). Thereafter, the membranes were incubated overnight at 4°C with 1 µg/ml rabbit anti-InsR for the detection of insulin receptor. On the following day, the membranes were washed four times with TBST and incubated at room temperature for 1 h with a HRP-conjugated anti-rabbit antibody (LiCor Bioscience) in 1:50000 as the secondary antibody. The mouse anti-actin antibody (1:1000) and the HRP-anti-mouse antibody (1:50000) (LiCor Bioscience) were used for the actin detection. For the enhanced chemiluminescence detection the SuperSignal West Femto Chemiluminescent Substrate (Thermo Scientific) was used and the ECL signal was recorded with the C-DiGit Blot Scanner (LiCor Bioscience). The quantification of the signal intensity was carried out with the Image Studio software (LiCor Bioscience).

Statistic analysis

All values of in vitro tests were expressed as the mean ± SD. The significance was analyzed with one-way ANOVA. The comparison between groups was performed with the unpaired two-tailed Student's t-test.

Results and Discussion

The average size of siRNA molecules is roughly at the upper limit of the size of the apoferritin cavity [27]. As illustrated in **Figure 1a**, once siRNA is encapsulated into apoferritin through disassembly and reassembly of the protein cage, the molecular composite resembles a virus-like structure without being a virus at all. This structure is expected to provide an efficient protection of siRNA from digestion by RNA degrading enzymes, for example RNase A. In fact, the enzymatic degradation can be used to evaluate the encapsulation efficiency.

With a diameter of 8 nm the apoferritin cage is large enough to host at least one single siRNA molecule. In order to ensure efficient encapsulation, siRNA in 3, 5 and 10-fold excess over apoferritin was used in our experiments. The encapsulation was accomplished through mixing the disassembled apoferritin with a concentrated siRNA solution at pH 8. In order to confirm successful encapsulation and compare the efficiency, half of the final mixture was initially treated with RNase A to digest the non-encapsulated siRNA and followed with digestion of the RNase with proteinase K to interrupt the digestion of the siRNA. The apoferritin is known for its resistance against proteinase K [28]. The amount of siRNA that remained after the treatment was compared with that present in the untreated mixture. Figure 1b (upper panel) shows that the encapsulation procedure itself did not affect the intactness of the siRNA. In a sample prepared with a 3:1molar ratio of apoferritin/siRNA, only approximately 50% of the siRNA was protected from the RNase A digestion. After increasing the ratio to 5:1 or above, over 95% siRNA remained intact after the enzyme digestion (Figure 1b). Mixing intact (already assembled) human H-chain apoferritin (apo-huFH) with siRNA did not prevent the enzymatic degradation of siRNA (Figure 1b, lower panel), which confirms that the earlier mentioned protection of siRNA is due to the encapsulation. No obvious differences in the encapsulation efficiency were observed between H- or L-chain apoferritin (Figure 1b, lower panel).

The disassembly-reassembly route has already been reported for the encapsulation of small molecules, even negatively charged solid inorganic nanoparticles into apoferritin [29]. The dependence of the encapsulation efficiency on the molar ratio of the components indicated that the encapsulation is a statistic event. However, the net surface charge of apoferritin changes from negative to positive once the pH is decreased below 5 (Supplementary Figure S1). At pH 2 the positive net charge will attract the negatively charged RNA molecules and upon reassembly may enhance the probability of an encapsulation. The cage-like structure of apoferritin remained intact after the encapsulation of siRNA (Figure 1c and Figure S2). The natural stability of apoferritin (especially apo-huFH) even preserved the encapsulated siRNA

in a serum-supplemented medium at 37 °C for 24 hours, which provides extraordinary protection of siRNA against endonucleases in vivo (Figure S3). Encapsulated siRNA can be stored in solution at 4 °C for at least four weeks without showing any detectable leakage or degradation (Figure S4). It is worth mentioning that these observations are by themselves of paramount importance as they open a completely new perspective for the use of apoferritin as safe and practical support for drug manufacturing, storage and transport.

The RNase-resistance of apoferritin-encapsulated siRNA is a key issue for the simple and cost-effective laboratory use of the composite for gene silencing, avoiding tedious sample preparation and medium exchange. We tested the efficiency upon cellular delivery in vitro by supplementing apo-huFH-encapsulated Cy3 conjugated siRNA (Cy3-siRNA) directly to cells in normal medium. The composite provided excellent cellular delivery not only in Caco-2 cells but also in HepG2 cells that are known to be difficult to become transfected (Figure 2a and Figure S5) [30]. In order to show the efficiency in gene silencing, the cells were treated with siRNA against insulin receptor (InsR) encapsulated in apo-huFH and –huFL. The commercial transfection agent Lipofectamine 3000 was used as reference. Since the half-life of InsR is around 6-7-h, the protein level of InsR was analyzed after 12 h treatment [31]. An 85% knockdown of InsR was achieved with apo-huFH as delivery agent, a 70% knockdown with apo-huFL, while only 40% silencing was achieved with Lipofectamine (Figure 2b). Commonly, serum-free medium is recommended for the use of Lipofectamine, thus the presence of serum in our experiments was possibly the main reason for its reduced efficiency in silencing. In addition, the transfection time (12 h) and the concentration of siRNA (10 nM) used in our experiments may not be optimal for Lipofectamine. The reason for the enhanced silencing efficiency with apo-huFH over apo-huFL may be found in the higher stability of the H-chain composite (Figure S3) and in its preferred cellular uptake through transferrin receptor-1, the major receptor for the uptake of extracellular ferritin [32].

Recently it has been demonstrated that H-chain ferritin is capable of quick nuclear translocation, which enables a nuclear DNA-targeted drug delivery [33, 34]. In order to verify whether or not this also applies to siRNA delivery, the lysosomes of Caco-2 cells were detected after a short-term (15 min.) and a long-term (24 h) treatment with a FITC-siRNA encapsulated in apo-huFH. The uptake and translocation of FITC-siRNA was rapid and after 15 minutes FITC-siRNA was clearly found inside the nuclei (Figure 3). Even the siRNA molecules present in the cytosol were not co-localized with the lysosomes after such short-term treatment. Since siRNA does not function inside nuclei, its accumulation in the nuclei may interfere with the desired gene silencing and may even be toxic to the cells. However, such risks may be ruled out after our observation where after 24 h huFH-delivered siRNA molecules were dominantly found in the cytosol (Figure 3). Obviously, the initially nuclear translocated molecules were either transported back into the cytosol or degraded in situ. Although the huFH-mediated nuclear translocation is not a requirement for siRNA function, it may support the encapsulated siRNA to escape from lysosomal degradation after the endocytosis, since the siRNA in the cytosol was still not associated with the lysosomes, even after 24 h (Figure 3). The mechanism still requires in-depth investigation, but the nuclear translocation can be considered as an important factor for the better silencing effect with apo-huFH.

Regenerative medicine is strongly attracted by the possibilities of steering gene expression of stem cells with siRNA [35]. Manipulating T-cell functions with siRNA is regarded to as a therapeutic strategy with exceptional promise for the treatment of cancer, infection and inflammatory diseases as well as HIV infection [1,3,36]. However, siRNA delivery approaches which are efficient on adherent tumor cells often perform poorly on primary and non-adherent cells. In order to test whether or not our approach acts efficiently also on primary and non-adherent cells, we performed tests on human mesenchymal stem cells (hMSC) and primary T-cells stimulated from peripheral blood mononuclear cells (PBMCs). In the first instance, confocal microscopy confirmed an efficient cellular uptake of siRNA-huFH by both hMSCs

and T-cells (Figure 4a and 4b). No obvious cytotoxicity was observed in both cell types even after 48 h (Figure S6). The cellular uptake of siRNA-huFH was further analyzed and confirmed with flow cytometry, especially for the case of T-cells that have a rather low cytoplasm volume (Figure 4c). The incessant increase in intensity of the siRNA signal between 24 and 48 h indicates that the apo-huFH delivery is steady and continuous (Figure 4c). Within 24 h no differences were observed for the delivery of 350 nM or 87 nM siRNA to primary T-cells, which means that the concentration can be even further reduced by functional gene silencing (Figure S7).

Although the endogenous origin of apoferritin suggests biocompatibility and safety for human medicine, due to its recombinant nature it is still necessary to confirm that there is no cytotoxicity and no immune responses upon delivery, especially with T- and B-cells in PBMCs. The biocompatibility of apo-huFH was confirmed with the fact that the viability of PBMCs did not change upon application of 1.75 µM (ca. 0.85 mg/ml) apo-huFH within 72 h, which was the concentration used for the 350 nM siRNA delivery (Figure S8). The activation of immune cells was evaluated with the detection of the CD25 positive cell population during 72 hours, comparing with PBMCs stimulated with phytohemagglutinin (PHA). Figure 5a shows that the recombinant apo-huFH did not activate the immune cells within 72 hours, even without the purification step to remove possible endotoxins, which may originate from its bacterial recombinant host. An interesting side-observation was that apo-huFH showed anti-inflammatory effects by partially inhibiting the PHA-mediated stimulation, especially on T cells (Fig. 5a and S9). Whether or not this anti-inflammatory phenomenon is related to the regulation effects of apoferritin on the iron homeostasis needs further in-depth investigation [25]. Nevertheless, the results confirm the hitherto presumed immune safety for clinical use of ferritin.

The dose requirements of RNAi for clinical relevance are approximately 100 nM for in vitro and in the range of mg/kg for clinical applications [37,38]. Since good delivery efficiency was

observed with 87 nM siRNA, we further tested the delivery and gene silencing efficiency on PBMCs with siRNA concentrations as low as 10 nM. Different delivery efficiencies were observed on inactivated and PHA-activated PBMCs. Only around 30% resting PBMCs could be transfected, independent of the delivery agent and the siRNA concentration (Fig. 5b). However, after a 2-day stimulation with PHA more than 60% cells were transfected with 10 nM apo-huFH-encapsulated siRNA within further 24 hours. Since the cellular uptake of ferritin is dominantly mediated by transferrin receptors [32], our observations are in good agreement with earlier evidences that transferrin receptors are present only on 30-40% of normal PMBCs [39] and that their expression will be induced upon PHA stimulation, especially on T cells [40]. The delivery with Lipofectamine 3000, the synthetic agent, did not show any response to the immune cell activation and its delivery capacity was much lower than apo-huFH in the low siRNA concentration range (10 nM and 25 nM) (Fig. 5b).

Since apo-huFH mediated delivery reacts to the immune cell activation, we tested the efficiency of silencing with siRNA against an activation-related gene. The insulin receptor (InsR), which is important for the T cell differentiation, is absent on resting T cells but will be induced upon activation [41]. After the PHA stimulation Western blot analysis confirmed a more than 2-fold up-regulation of InsR on the whole PBMCs (Figure 5c). The silencing efficiency on resting PBMCs was around 30% with 10 nM siRNA against InsR, while a 70% silencing was achieved on the PHA-activated cells. Apo-huFH delivered InsR-siRNA reduced the receptor level of activated cells below the InsR level of resting cells. Upon increase of the siRNA concentration to 25 nM, the silencing was further enhanced by 5-10% (Figure 5c). Here again some mild InsR down-regulation effect was observed with apo-huFH on PBMCs. The silencing effects with siRNA-huFH outperformed those with lipofectamine in the evaluated concentration range. Similar with the observation from Caco-2 cells, lipofectamine is presumably not suitable for a use as delivery agent in the presence of serum in the medium, which will cause serious difficulties for its clinical use. The excellent delivery performance with lower siRNA

concentrations demonstrates that human ferritin is indeed superior to synthetic agents of clinical relevance.

As an interesting observation of this work, the enhanced delivery with apo-huFH to activated immune cells may shed some light on applications of ferritin-mediated delivery in real life conditions. Our experiments indicate that ferritin can deliver encapsulated drugs efficiently when activated immune cells are present (for example due to infections), while less effectively to non-activated cells. Strict cell selectivity in vivo may be difficult to achieve with the unmodified form of human ferritin due to the ubiquitously expressed transferrin receptor. For in vivo targeting, several modifications of ferritin have already been tested [20,22]. However, the demonstrated ferritin mediated delivery could prove very useful for manipulating isolated T-cells ex vivo, which is clinically approved as adoptive cell therapy [42].

In a nutshell, apoferritin-mediated siRNA delivery is an efficient method for applications to a broad cell population, at least for ex vivo transfection of primary and tumorigenic cells. All siRNAs are duplexes with ca. 21 nucleotides and all siRNAs for any gene of interest will have similar overall sizes, which match very well the restrictions posed by the cavity of apoferritin [43]. Since the encapsulation of siRNA into apoferritin is independent of its sequence, our approach shows enormous potential for the cellular delivery of siRNA to perform a variety of gene knockdown and silencing therapies. The endogenous origin and immune safety of apoferritin is a clear advantage over the commonly investigated or applied viral and synthetic agents. The observed natural selectivity of apoferritin-mediated delivery between inactivated and activated immune cells and also the possible anti-inflammatory effects of ferritin demonstrate that the unique biological functions of ferritin may help to achieve synergic effects in certain therapies, which is hardly imaginable from synthetic delivery agents.

Acknowledgements

M.K. and L.Z. greatly acknowledge financial support through Marie Curie Actions (CIG) within project number 322158 (ARTEN). The authors greatly acknowledge financial support by the Spanish Ministry of Economy and Competitivity (MINECO) through project number MAT2012-38161, the Diputación Foral de Guipúzcoa through project number DFG15/006, and the Basque Government through project number PI2013-56. The authors also acknowledge the Cell Culture Platform from Biodonostia Institute.

Competing interests
The authors declare no competing interests.

References

[1] B. L. Davidson, P. B. McCray Jr, *Nat. Rev. Genet.* 12 (2011) 329-340.

[2] J. K. Lam, M. Y. Chow, Y. Zhang, S. W. Leung, *Mol. Ther. Nucleic Acids* (2015) *4*:e252.

[3] P. Kumar, H. S. Ban, S. S. Kim, H. Wu, H. T. Pearson, D. L. Greiner, A. Laouar, J. Yao, V. Haridas, K. Habiro, Y. G. Yang, J. H. Jeong, K. Y. Lee, Y. H. Kim, S. W. Kim, M. Peipp, G. H. Fey, N. Manjunath, L. D. Shultz, S. K. Lee, P. Shankar, *Cell* 134 (2008) 577-586.

[4] A. Eguchi, B. R. Meade, Y. C. Chang, C. T. Fredrickson, K. Willert, N. Puri, S. F. Dowdy, *Nat. Biotechnol.* 27 (2009) 567-571.

[5] Y. Zhang, A. Satterlee, L. Huang, *Mol. Ther.* 20 (2012) 1298-1304.

[6] K. A. Whitehead, R. Langer, D. G. Anderson, *Nat. Rev. Drug. Discov.*8 (2009) 129-138.

[7] R. P. Hickerson, A. V. Vlassov, Q. Wang, D. Leake, H. Ilves, E. Gonzalez-Gonzalez, C. H. Contag, B. H. Johnston, R. L. Kaspar, *Oligonucleotides* 18 (2008) 345-354.

[8] Y. Gao, X. L. Liu, X. R. Li, *Int. J. Nanomed.* 6 (2011) 1017-1025.

[9] S. M. Moghimi, P. Symonds, J. C. Murray, A. C. Hunter, G. Debska, A. Szewczyk, *Mol. Ther.* 11 (2005) 990-995.

[10] P. Symonds, J. C. Murray, A. C. Hunter, G. Debska, A. Szewczyk, S. M. Moghimi, *FEBS Lett.* 579 (2005) 6191-6198.

[11] M. Sioud, *Methods Mol. Biol.* 1218 (2015) 1-15.

[12] L. K. Müller, K. Landfester, *Biochem. Biophys. Res. Commun.* (2015) pii: S0006-291X(15)30478-2.

[13] S. Somani, D. R. Blatchford, O. Millington, M. L. Stevenson, C. Dufès, *J. Control. Release* 188 (2014) 78–86.

[14] S. A. Kooijmans, S. Stremersch, K. Braeckmans, S. C. de Smedt, A. Hendrix, M. J. Wood, R. M. Schiffelers, K. Raemdonck, P. Vader, *J. Control. Release* 172 (2013) 229-238.

[15] L. Alvarez-Erviti, Y. Seow, H. Yin, C. Betts, S. Lakhal, M. J. Wood, *Nat. Biotechnol.* 29 (2011) 341-345.

[16] Y. Tian, S. Li, J. Song, T. Ji, M. Zhu, G. J. Anderson, J. Wei, G. Nie, *Biomaterials* 35 (2014) 2383-2390.

[17] K. B. Johnsen, J. M. Gudbergsson, M. N. Skov, L. Pilgaard, T. Moos, M. Duroux, *Biochim. Biophys. Acta.* 1846 (2014) 75-87.

[18] E. C. Theil, R. K. Behera, T. Tosha, *Coord. Chem. Rev.* 257 (2013) 579–586.

[19] L. Zhang, W. Fischer, E. Pippel, G. Hause, M. Brandsch, M. Knez, *Small* 7 (2011) 1538–1541.

[20] Z. Zhen, W. Tang, H. Chen, X. Lin, T. Todd, G. Wang, T. Cowger, X. Chen, J. Xie, *ACS Nano* 7 (2013) 4830-4837.

[21] P. Huang, P. Rong, A. Jin, X. Yan, M. G. Zhang, J. Lin, H. Hu, Z. Wang, X. Yue, W. Li, G. Niu, W. Zeng, W. Wang, K. Zhou, X. Chen, *Adv. Mater.* 26 (2014) 6401–6408.

[22] K. Fujita, Y. Tanaka, S. Abe, T. Ueno, *Angew. Chem. Int. Edit.* 55 (2016) 1056-1060.

[23] G. Jutz, P. van Rijn, B. Santos Miranda, A. Böker, *Chem Rev.* 115 (2015) 1653-701.

[24] C. Cao, X. Wang, Y. Cai, L. Sun, L. Tian, H. Wu, X. He, H. Lei, W. Liu, G. Chen, R. Zhu, Y. Pan, *Adv. Mater.* 26 (2014) 2566-2571.

[25] L. Li, L. Zhang, U. Carmona, M. Knez, *Chem. Commun.* 50 (2014) 8021-8023.

[26] E. J. Lee, S. J. Lee, Y. S. Kang, J. H. Ryu, K. C. Kwon, E. Jo, J. Yhee, I. C. Kwon, K. Kim, J. Lee, *Adv. Funct. Mater.* 25 (2015) 1279–1286.

[27] P. Guo, O. Coban, N. M. Snead, J. Trebley, S. Hoeprich, S. Guo, Y. Shu, *Adv. Drug Deliv. Rev.* 62 (2010) 650–666.

[28] B.G. Atkinson, R.L. Dean, J. Tomlinson, T.W. Blaker, Biochem. Cell Biol. 67 (1989) 52-57.

[29] J. C. Cheung-Lau, D. Liu, K. W. Pulsipher, W. Liu, I. J. Dmochowski, *J. Inorg. Biochem.* 130 (2014) 59-68.

[30] E. T. Jordan, M. Collins, J. Terefe, L. Ugozzoli, T. Rubio, *J. Biomol. Tech.* 19 (2008) 328-334.

[31] B. C. Reed, G. V. Ronnett, P. R. Clements, M. D. Lane, *J. Biol. Chem.* 256 (1981) 3917-3925.

[32] L. Li, C. J. Fang, J. C. Ryan, E. C. Niemi, J. A. Lebrón, P. J. Björkman, H. Arase, F. M. Torti, S. V. Torti, M. C. Nakamura, W. E. Seaman, *Proc. Natl. Acad. Sci. U. S. A.* 107 (2010) 3505.

[33] M. Bellini, S. Mazzucchelli, E. Galbiati, S. Sommaruga, L. Fiandra, M. Truffi, M. A. Rizzuto, M. Colombo, P. Tortora, F. Corsi, D. Prosperi, *J. Control. Release* 196 (2014) 184-196.

[34] L. Zhang, L. Li, A. Di Penta, U. Carmona, F. Yang, R. Schöps, M. Brandsch, J. L. Zugaza, M. Knez, *Adv. Healthc. Mater.* 4 (2015) 1305-1310.

[35] S. M. Millard, N. M. Fisk, *Bioessays* 35 (2013) 173-182.

[36] M. Freeley, A. Long, *Biochem. J.* 455 (2013) 133-147.

[37] T. Martínez, M. V. González, I. Roehl, N. Wright, C. Pañeda, A. I. Jiménez, *Mol. Ther.* 22 (2014) 81-91.

[38] X. J. Li, Z. J. Ren, J. H. Tang, *Cell Death Dis.* (2014) 5:e1327.

[39] S. Kinik, M. A. Tuncer, F. Gümrük, A. Gürgey, C. Altay, *Pediatr. Res.* 45 (1999) 760.

[40] E. Pelosi, U. Testa, F. Louache, P. Thomopoulos, G. Salvo, P. Samoggia, C, Peschle, *J. Biol. Chem.* 261 (1986) 3036-3042.

[41] A. Viardot, S. T. Grey, F. Mackay, D. Chrisholm, *Endocrinology* 148(2007) 346-353.

[42] N. P. Restifo, M. E. Dudley, S. A. Rosenberg, *Nat. Rev. Immunol.* 12 (2012) 269-281.

[43] S. M. Elbashir, *Genes Dev.* 15 (2001) 188–200.

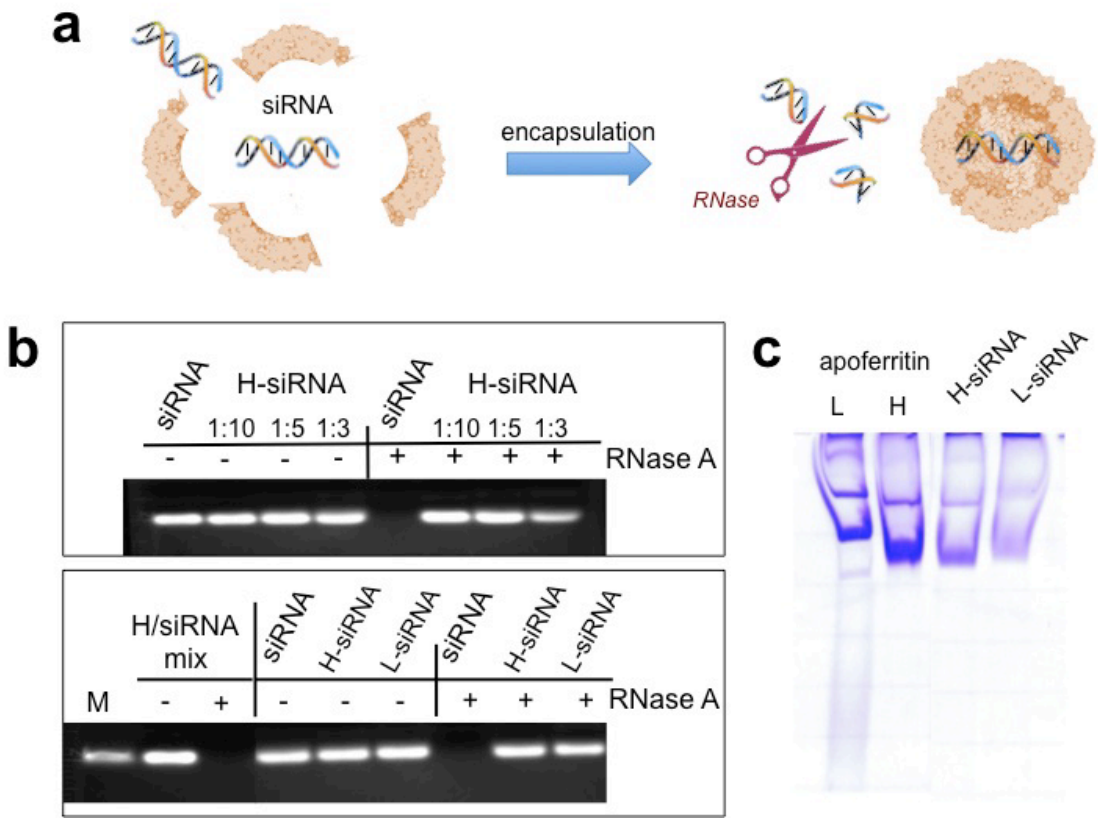

Figure 1. Efficient encapsulation and protection of siRNA in human apoferritin. (a), Schematic presentation of the encapsulation process and protection of siRNA inside the apoferritin cavity. **(b)**, Encapsulation efficiency with various siRNA/apo-huFH ratios (upper panel) and the stability of encapsulated siRNA in apo-huFH and –huFL (H-siRNA and L-siRNA, respectively) at room temperature for 24 h (lower panel). siRNA against insulin receptor and Cy3-modified siRNA were used for the experiments shown in the upper and lower panel, respectively. H/siRNA mix: simple mixture of intact apo-huFH with M: molecular weight marker. For the RNase A digestion assay, each sample with 0.5 µg siRNA was incubated with 0.5 µg/ml RNase A followed by digestion with 0.5 mg/ml proteinase K in order to interrupt the RNase A activity. **(c)**, Characterization of the reassembly of protein cage of apoferritin after siRNA-encapsulation with 4% continuous native gel electrophoresis.

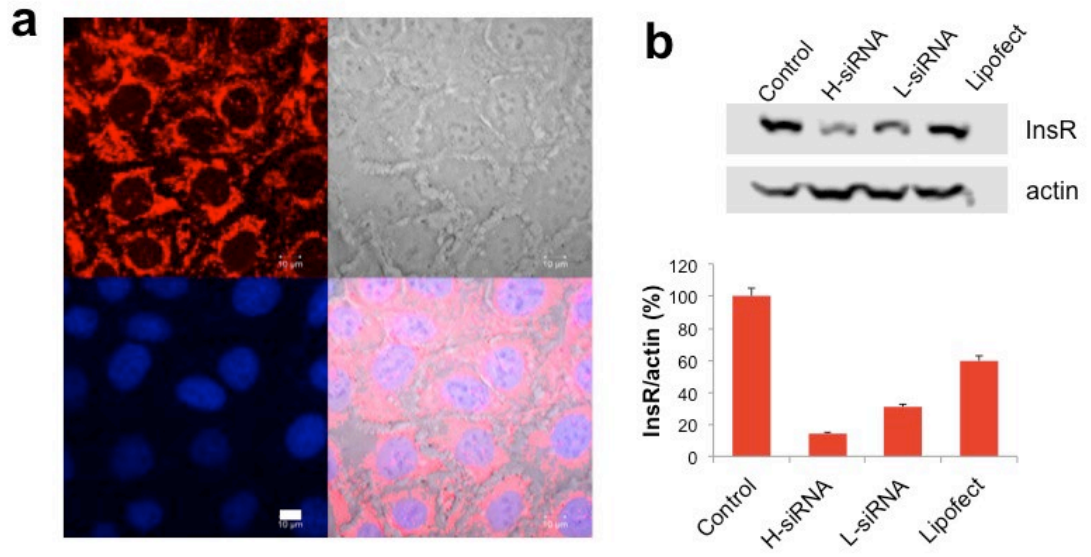

Figure 2. Highly efficient siRNA delivery and gene silencing in Caco-2 cells. (a), Live cell imaging of Caco-2 cells treated with 350 nM Cy3-siRNA (red) encapsulated in human H-apoferritin for 24 h. The nuclei were stained with Hoechst 33342 staining (blue). Scale bar: 10 μm. **(b),** Western blot detection and quantification of the insulin-receptor (InsR) after 12 h treatment with 10 nM siRNA against InsR with human H- and L-chain apoferritin, and Lipofectamine 3000 as the delivery agents (H-siRNA, L-siRNA and Lipofect, respectively). Cells without siRNA treatment were used as control (Control). Actin was detected as the loading control. The intensity ratio of InsR/actin of the control cells was set as 100%. The quantification results are shown as value ± SD. The treatment was carried out in normal medium with 10% FBS.

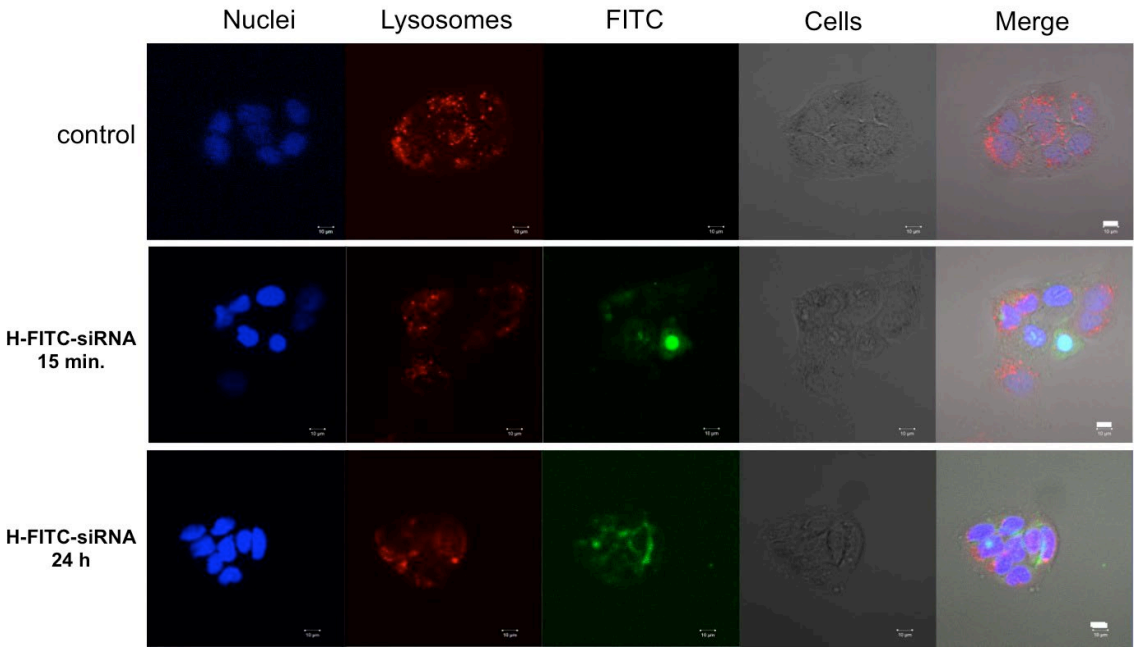

Figure 3. Location of siRNA and lysosomes in Caco-2 cells. Live cell imaging of Caco-2 cells treated with 100 nM H-FITC-siRNA (green) encapsulated in human H-apoferritin for 15 min. and 24 h. The nuclei were stained with Hoechst 33342 (blue). Cells pretreated with 150 µM chloroquine for 2h were used as control (control). Lysosomes were stained with the Lyso-ID® red dye. All treatments were carried out in normal medium with 10% FBS. Scale bar: 10 µm.

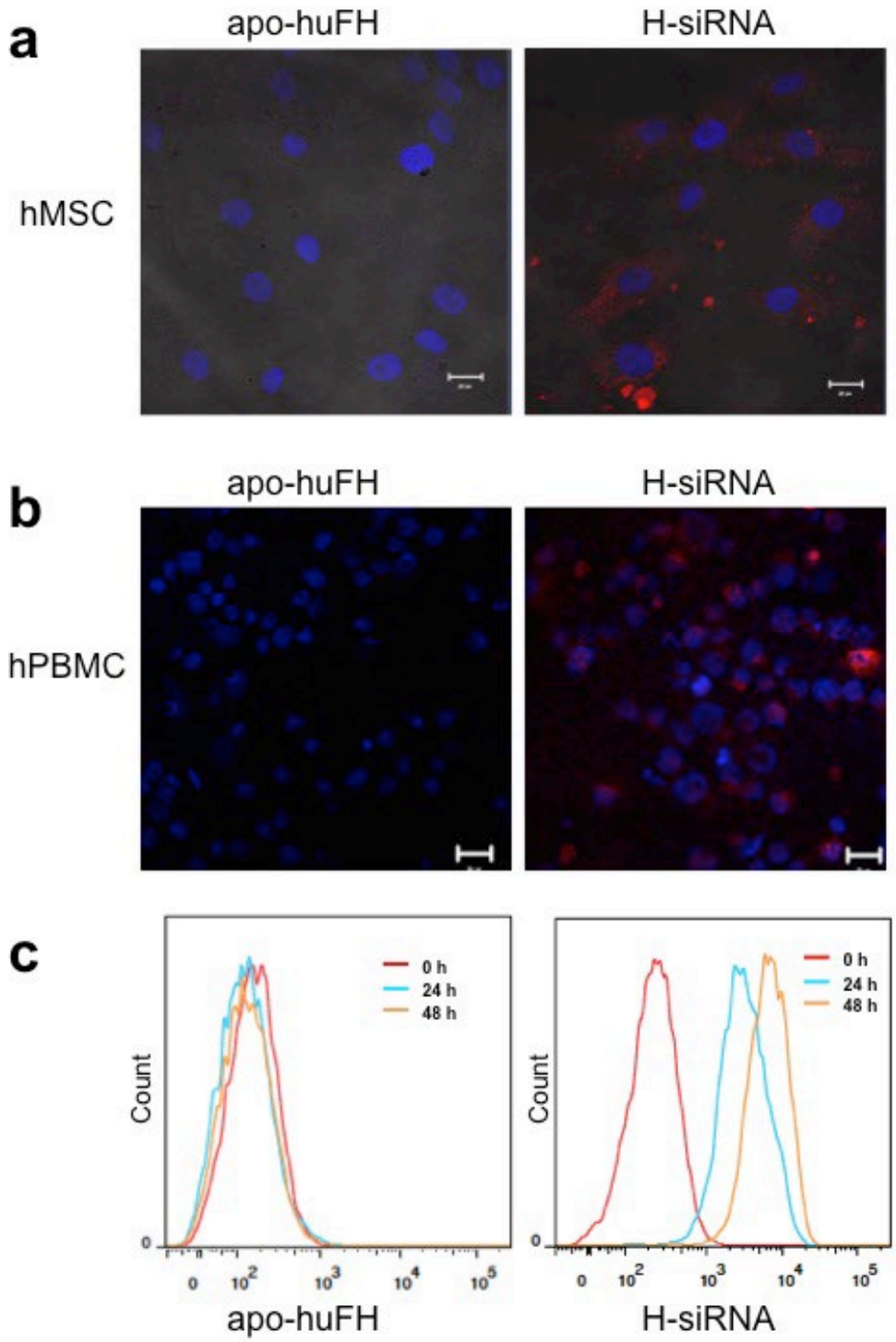

Figure 4. Highly efficient siRNA delivery in human primary cells. Live cell imaging of **(a),** human mesenchymal stem cells (hMSC) and **(b),** human primary T-cells stimulated from peripheral blood mononuclear cells (PBMCs) treated with H-siRNA (350 nM Cy3-siRNA (red) encapsulated in human H-apoferritin) and apo-huFH for 24 h. The nuclei were stained with DAPI (blue). Scale bar: 20 μm. **(c),** Flow cytometry analysis of the uptake of 350 nM Cy3-siRNA encapsulated in human H-apoferritin (H-siRNA) in primary T-cells during 48 h. All treatments of the primary cells were carried out in normal medium with 10% FBS.

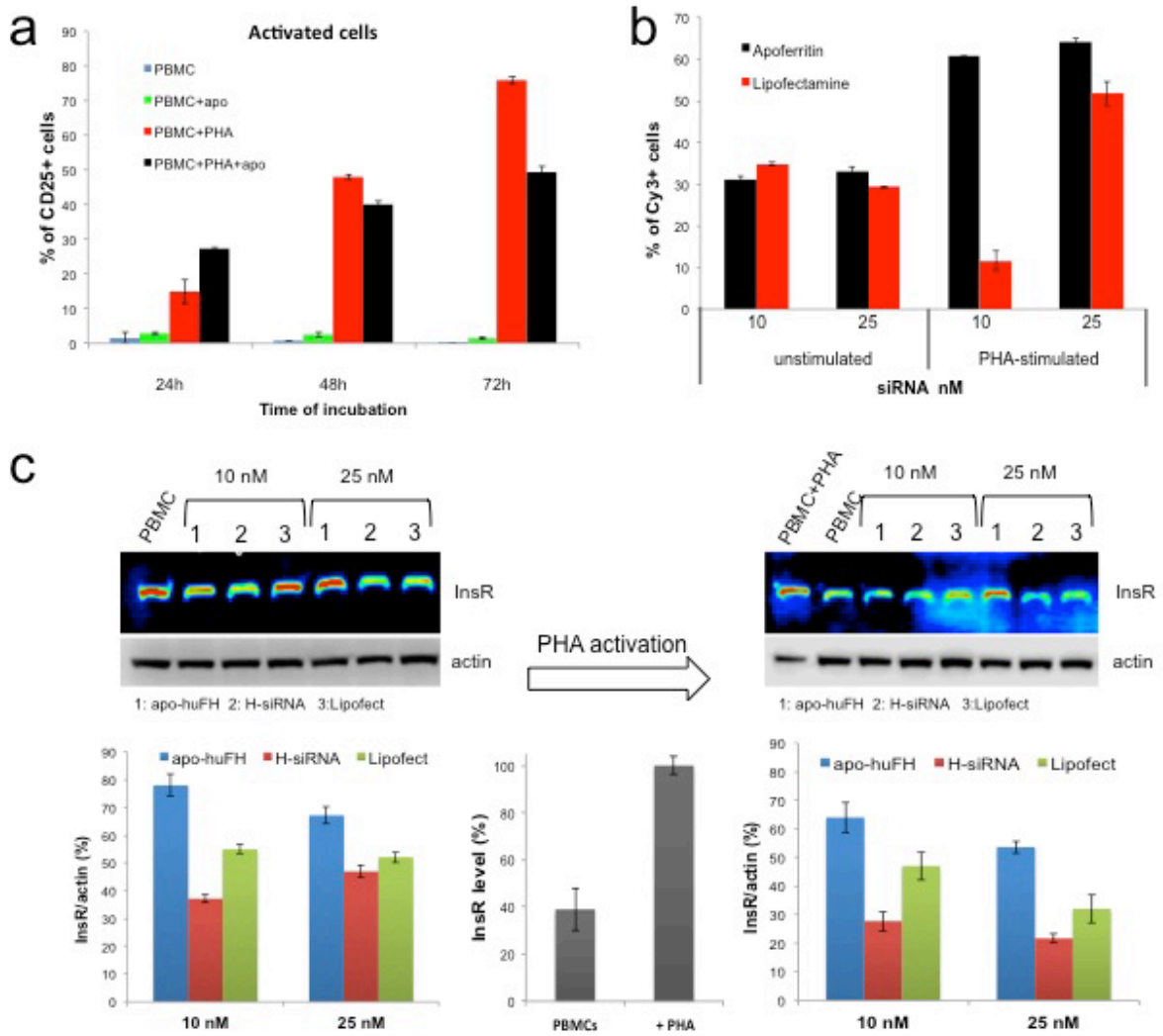

Figure 5. Efficient siRNA delivery and gene silencing in human PBMCs. (a), Flow cytometry analysis of the effects of H-chain apoferritin (apo) on the activation of PBMCs within 72 hours. Effects of 1.75 μM apo-huFH were compared with the activation with 0.5% phytohemagglutinin (PHA). CD25 was detected as the marker for the activation. **(b),** Flow cytometry analysis of the delivery efficiency of 10 and 25 nM Cy3-siRNA with apo-huFH and lipofectamine 3000 on both unstimulated and PHA-stimulated PBMCs. **(c),** Western blot analysis and quantification of the insulin receptor (InsR) expression level of human PBMCs with or without PHA stimulation. 10 and 25 nM siRNA against InsR were delivered either in human H-apoferritin (H-siRNA) or with lipofectamine 3000 (Lipofect). Cells treated with human H-apoferritin (apo-huFH) serve as the vehicle control. The intensity ratio of InsR/actin of PBMCs with or without PHA stimulation was set as 100% for quantification. The quantification results are shown as value ± SD.

Supporting Information

Ferritin-Mediated siRNA Delivery and Gene Silencing in Human Tumor and Primary Cells

Le Li, Maider Muñoz Culla, Unai Carmona, Maria Paz Lopez, Fan Yang, Cesar Triguero, David Otaegui, Lianbing Zhang, and Mato Knez**

Additional Materials and Methods

Human primary cells

Blood samples and data from patients included in this study were provided by the Basque Biobank for Research-OEHUN (www.biobancovasco.org) and were processed following standard operating procedures. Peripheral Blood Mononuclear Cells (PBMCs) were purified from Buffy Coat by density gradient using Lymphoprep (ATOM, 50898). Once isolated, the PBMCs were frozen for preservation until use in subsequent experiments. PBMCs were activated with "Dynabeads® Human T-Activator CD3⁄CD28" (Life Technologies, 11131D) plus IL-2 (10 ng/ml, R&D). A *ratio* of 1:1 of CD3/CD28 beads to PBMCs was used as recommended by the manufacturer. PBMCs were cultured in RPMI supplemented with 10% FBS. At 0 time point, apoferritin or apoferritin encapsulated Cy3-siRNA were added to a final concentration of 350 nM siRNA and the fluorescence was analyzed at 0, 24, 48 h time points. FACS analysis was carried out in a BD FACSaria II (Becton Dickinson) using excitation laser 561 nm; The light was collected with a 610/20 BP filter. Data analysis was done using BD FACSDIva software (Becton Dickinson). Dead cells were excluded using Topro-3 (Lifetechnologies) and doublets were excluded as well from the analysis. For fluorescence microscopy, PBMCs cells were included in a slide by cytospin, Fixed PFA 4% and stained with mounting media (Prolongold+DAPI, Lifetechnologies).

Human bone marrow–derived Mesenchymal SCs (MSCs) were obtained from the Inbiobank Stem Cell Bank (www.inbiobank.org). Briefly, cadaveric bone marrow was harvested from

brain-dead donors after informed consent and under the Spanish National Organization of Transplant supervision (*Organización Nacional de Transplantes*, ONT). Generated MSCs display a typical CD29+, CD73+, CD90+, CD105+, CD166+, CD146+, CD34-, CD45–, CD14–, CD19–, and CD31– phenotype; a fibroblast-like morphology; and at least trilineage potential, including osteocyte, chondrocyte, and adipocyte generation. MSCs were cultured in low-glucose DMEM supplemented with 10% FBS. On reaching confluence, MSCs were trypsinized and seeded at a density of $1x10^3$ cells/cm^2. Cells were obtained at passage three from the Stem Cell Bank. MSC were cultured on 8-wells chamber slides (Lab-Tek Nalgene). After adding apoferritin or apoferritin encapsulated Cy3-RNAi, fluorescence microscopy was performed at 0, 24, 48 hours using Cy3 filter set 00 (Zeiss) in a Axiobserver A1 microscope. For f M the samples, MSc were fixed PF 4% and mounting media (Prolongold +DAPI, Lifetechnologies).

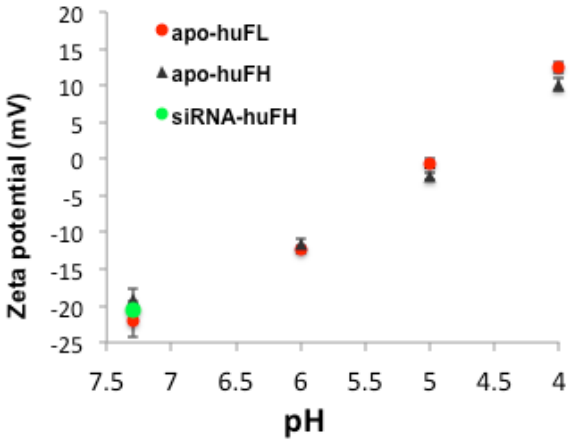

Fig. S1. Zeta potential of apo-huFL or –huFH at pH 7.3, 6, 5, and 4. The Zeta potential of apo-huFH shows no change after the siRNA encapsulation (siRNA-huFH).

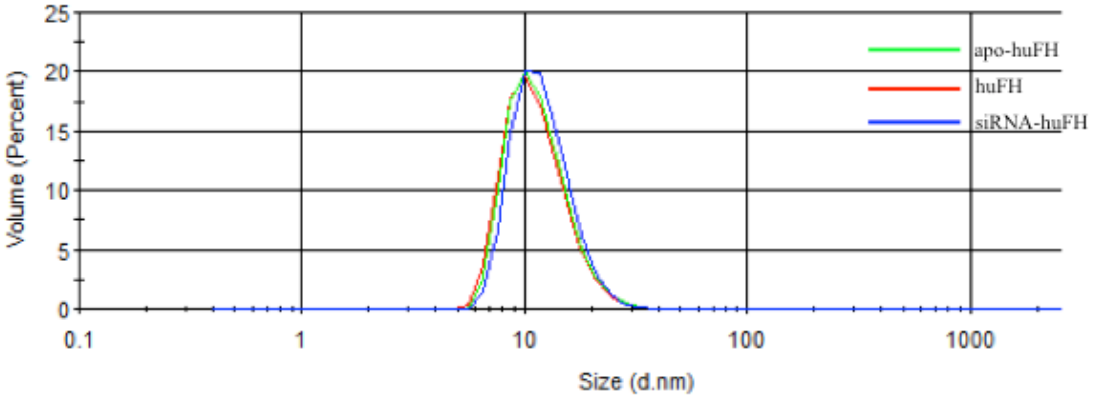

Fig. S2. Size distribution of human H-chain apoferritin (apo-huFH), human H-chain ferritin (huFH), and apo-huFH with encapsulated siRNA (siRNA-huFH). Measured with ZetaSizer.

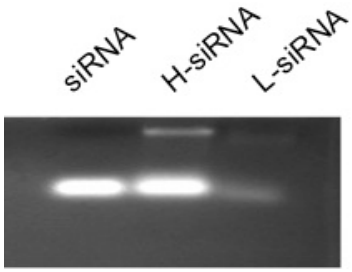

Fig. S3. Stability of apoferritin encapsulated siRNA in serum-supplemented medium. 0.5 μg siRNA was encapsulated in apo-huFL or –huFH (L-siRNA or H-siRNA), and then incubated in cell medium with 10% fetal bovine serum 24 h at 37 °C. The samples were then digested with 0.5 μg/ml RNase A followed by 0.5 mg/ml Proteinase K. The presence of intact siRNA was visualized on 1% agarose gel. 0.5 μg bare siRNA was loaded for comparison.

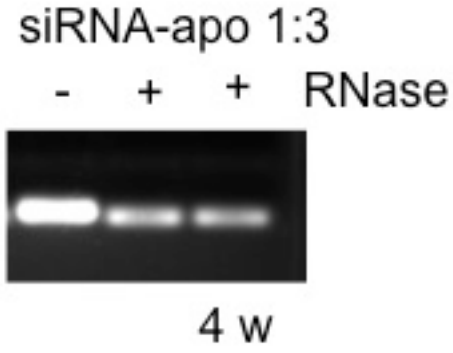

Fig. S4: Stability of apoferritin encapsulated siRNA in aqueous solution. 0.5 μg siRNA was encapsulated in apo-huFH with a molar ratio of siRNA/apoferritin of 1:3 (siRNA-apo), and then stored as prepared at 4 °C for 4 weeks. The samples were then digested with 0.5 mg/ml Proteinase K. The presence of intact siRNA was visualized on 1% agarose gel. 0.5 μg bare siRNA and freshly prepared siRNA-apo was loaded for comparison.

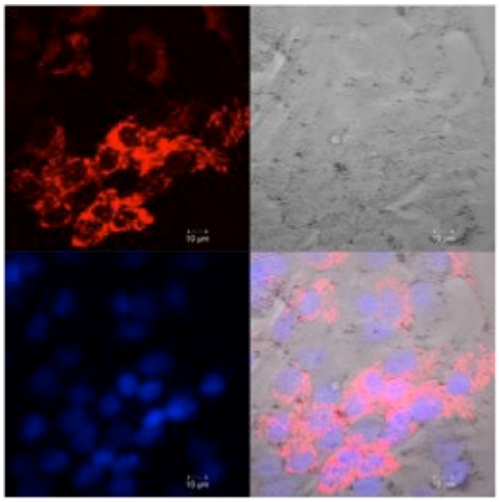

Fig. S5: Highly efficient siRNA delivery and gene silencing in HepG2 cells. (a), Live cell imaging of HepG2 cells treated with 350 nM Cy3-siRNA (red) encapsulated in human H-apoferritin for 24 h. The nuclei were stained with Hoechst 33342 (blue). Scale bar: 10 µm.

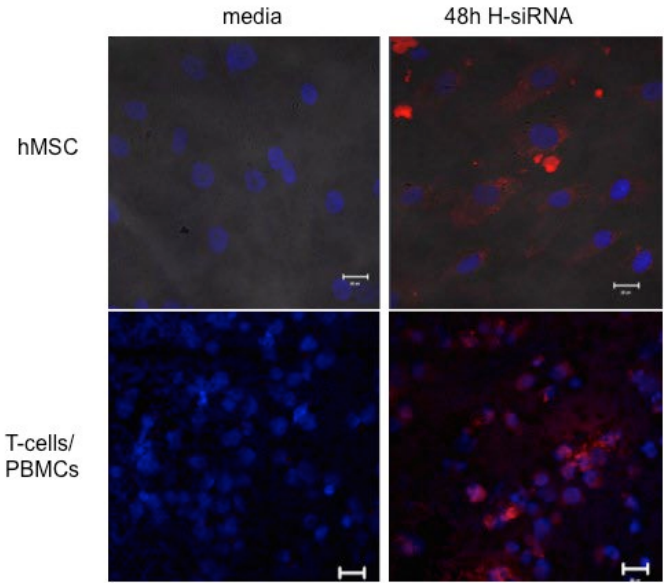

Fig. S6: Highly efficient siRNA delivery in human primary cells. Live cell imaging of human mesenchymal stem cells (hMSC) and human primary T-cells stimulated from peripheral blood mononuclear cells (PBMCs) treated 48 h with H-siRNA (350 nM Cy3-siRNA in human H-apoferritin) and untreated cells (media). The nuclei were stained with DAPI (blue). Scale bar: 20 µm.

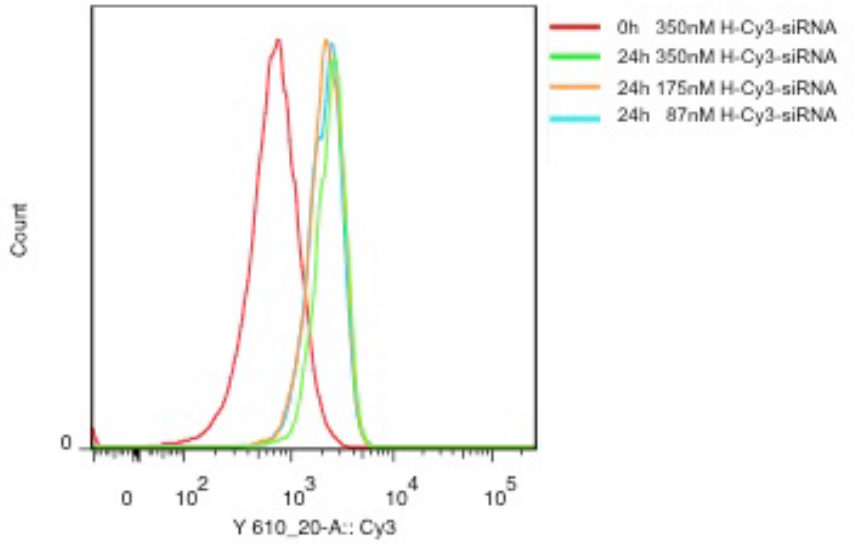

Fig. S7: Highly efficient siRNA delivery in human primary T-cells. Flow cytometry analysis of uptake of 350, 175, and 87 nM Cy3-siRNA encapsulated in human H-apoferritin (H-Cy3-siRNA) in primary T-cells within 24 h. All treatments of the primary cells were carried out in normal medium with 10% FBS.

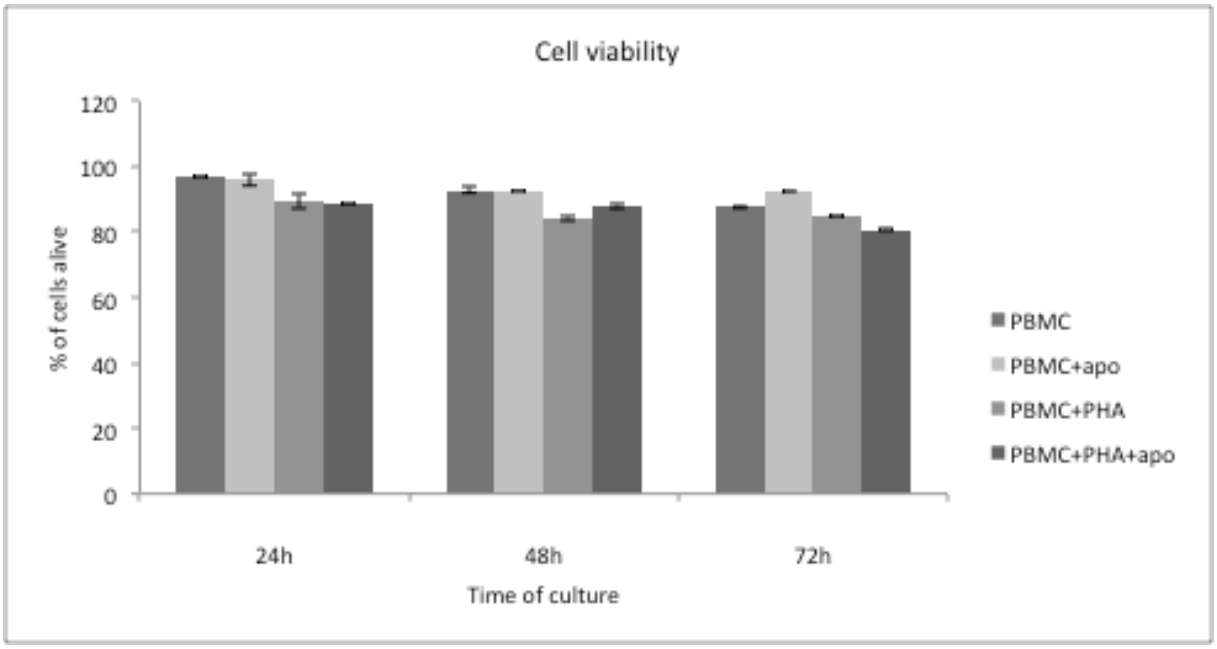

Fig. S8: Effect of apo-huFH on the viability of PBMCs. Flow cytometry analysis of the cell viability upon treatment with 1.75 µM apo-huFH. The viability of normal PBMCs and the PHA-stimulated cells were measured for comparison.

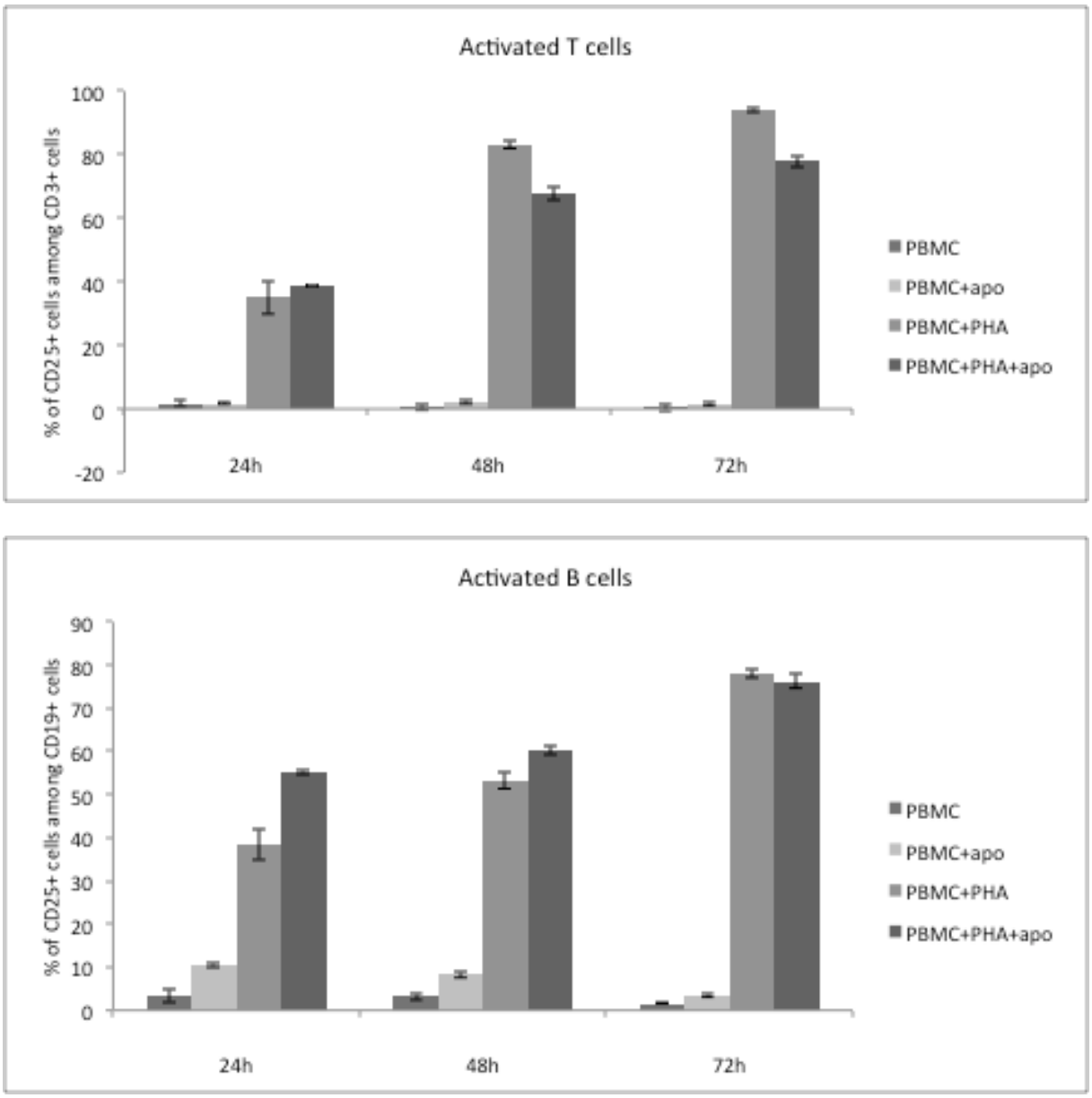

Fig. S9: Effect of apo-huFH on immune-activation of PBMCs. Flow cytometry analysis of the activation of T-cells (CD3 positive) and B-cells (CD19 positive) in PBMCs with CD25 as marker for the activation (with 0.5% phytohemagglutinin (PHA)). 1.75 µM apo-huFH was added by the incubation.